A generalized marginal stability criterion for shear-induced ocean interior diapycnal turbulent mixing

Ali Mashayek[1,1], Colm Caulfield[2,2], Lois Baker[1,1], and B. B. Cael[3,3]

[1]Imperial College London
[2]University of Cambridge
[3]National Oceanography Centre

November 30, 2022

Abstract

Turbulent mixing induced by breaking internal waves is key to the ocean circulation and global tracer budgets. While the classic marginal shear instability of Richardson number 1/4 has been considered as potentially relevant to turbulence wave breaking, its relevance to energetic zones where tides, winds, and buoyancy gradients excite non-linearly interacting processes has been suspect. We show that shear instability is indeed relevant in the ocean interior and propose an alternative generalized marginal stability criterion, based on the ratio of Ozmidov and Thorpe turbulence scales, which not only applies to the ocean interior, but remains relevant within turbulent boundary layers. This allows for accurate quantification of the transition from downwelling to upwelling zones in a recently emerged paradigm of ocean circulation. Our results help climate models more accurately calculate the mixing-driven deep ocean circulation and fluxes of tracers in the ocean interior.

A generalized marginal stability criterion for shear-induced ocean interior diapycnal turbulent mixing

A. Mashayek[1]*, L. E. Baker[1], B.B. Cael[2], and C. P. Caulfield[3]

[1]Imperial College London
[2]National Oceanography Centre Southampton
[3]University of Cambridge

Key Points:

- Intermittent turbulence emerges in a marginally stable ocean interior by localized bursts in shear.
- Data suggests shear instability is the prevalent facilitator of turbulence, even close to boundaries.
- The marginally unstable turbulent patches seem to mix optimally during most of their life cycles.

*The last three authors are listed in alphabetical order.

Corresponding author: Ali Mashayek, mashayek@imperial.ac.uk

Abstract

Turbulent mixing induced by breaking internal waves is key to the ocean circulation and global tracer budgets. While the classic marginal shear instability of Richardson number $\sim 1/4$ has been considered as potentially relevant to turbulence wave breaking, its relevance to energetic zones where tides, winds, and buoyancy gradients excite nonlinearly interacting processes has been suspect. We show that shear instability is indeed relevant in the ocean interior and propose an alternative generalized marginal stability criterion, based on the ratio of Ozmidov and Thorpe turbulence scales, which not only applies to the ocean interior, but remains relevant within turbulent boundary layers. This allows for accurate quantification of the transition from downwelling to upwelling zones in a recently emerged paradigm of ocean circulation. Our results help climate models more accurately calculate the mixing-driven deep ocean circulation and fluxes of tracers in the ocean interior.

Plain Language Summary

Internal waves induced by tides, winds, currents, eddies, and other processes abound in the ocean interior. Widespread breaking of internal waves, similar to surface coastal waves, plays an important role in sustaining the ocean circulation by upwelling the densest waters that form in polar regions and sink to the ocean abyss as well as in transport and storage of heat, carbon, and nutrients. In this work, we show how a well-understood classic hydrodynamic instability facilitates such wave breaking on the global scale in such a fashion that keeps the turbulent mixing induced by breaking waves optimally efficient.

1 Introduction

Breaking internal waves induce widespread turbulent mixing at all ocean depths and across the globe, thereby playing an important role in (I) closure of the ocean circulation by upwelling of dense waters that form in polar regions and sink to the abyssal ocean basins and (II) regulating the budgets of heat, carbon, nutrients and other tracers important to the climate system (Wunsch & Ferrari, 2004; Talley et al., 2016). Internal waves are forced at both surface and bottom ocean boundaries through winds, tides and ocean currents and eddies (Garrett & Kunze, 2007; Nikurashin & Ferrari, 2013; Legg, 2021; Alford, 2020). They can also be internally forced due to interaction of currents and eddies or directly through hydrodynamic instabilities that arise due to enhanced vertical gradient or 'shear' of horizontal velocity (S. A. Thorpe, 2005).

Dating back to the pioneering work of G. I. Taylor, it has long been known that under certain circumstances, locally enhanced vertical shear in a stratified fluid leads to an array of flow instabilities that can trigger the transition to turbulence and (ultimately) irreversible mixing. A key controlling parameter for stratified shear flows is the (gradient) Richardson number $Ri(z,t)$, the ratio of the square of the buoyancy frequency N and the background vertical shear S:

$$Ri(z,t) := \frac{N^2}{S^2};\ N^2 := -\frac{g}{\rho_0}\frac{\partial}{\partial z}\overline{\rho}(z,t);\ S := \frac{\partial}{\partial z}\overline{U}(z,t), \tag{1}$$

where g is the acceleration due to gravity, ρ_0 is a reference density, and $\overline{\rho}(z,t)$ and $\overline{U}(z,t)$ are appropriate averages of the density and horizontal velocity.

In two classic papers, Miles (1961); Howard (1961) established that a necessary condition for flow instability in a laminar steady inviscid shear layer is that $Ri < Ri_L = \frac{1}{4}$ somewhere within the layer, where the flow is linearly marginally stable.Although the proof of this result is essentially mathematical for a very idealized flow situation, many studies (and indeed parameterizations) have been based around heuristic ener-

getic arguments leading to the criterion that $Ri(z,t) \lesssim Ri_L$ somewhere is a necessary condition for sustained turbulence within a flow. In practice, the specific theoretical value of $Ri = Ri_L = \frac{1}{4}$ associated with the linear stability theory of laminar flow is identified as being a marginal Richardson number Ri_m for the existence of sustained turbulence.

Turner (1979) argued that stratified shear flows can naturally adjust into a 'kind of equilibrium' where local (in space and/or time) intensification of shear will lead to a local drop in Ri, allowing instability, enhanced turbulent dissipation and hence reduction in the shear until the flow becomes at least close to an attracting state of marginal stability. In an analogous fashion, S. A. Thorpe and Liu (2009) argued that generically stratified shear flows will adjust towards a state of such 'marginal instability', with $Ri \simeq Ri_m \simeq Ri_L = \frac{1}{4}$.

Such a tendency to converge towards marginal stability has some connection with the more general physical concept of 'self-organized criticality' (SOC) within a dynamical system, as originally argued by Bak et al. (1987). Salehipour et al. (2018) presented detailed numerical evidence suggestive of SOC in flows susceptible to the inherently stratified 'Holmboe Wave Instability', which typically occurs when a relatively sharp density interface is subject to relatively more vertically extended shear, while W. D. Smyth et al. (2019) argued that SOC was more generally characteristic of shear-driven turbulence in both simulation and real oceanic flows.

Indeed, as originally shown by Woods (1968) by direct dye measurements in the Mediterranean, and subsequently in many observational studies (see for example van Haren and Gostiaux (2010); Geyer et al. (2010)), vortical structures at least visually reminiscent of the classic shear-driven overturning 'Kelvin-Helmholtz' instability appear to play an important role in turbulent mixing in the world's oceans, and observational measurements of Richardson number have also been shown to be peaked around the theoretical linear stability value of $Ri_L = \frac{1}{4}$ in various oceanic environments (W. D. Smyth & Moum, 2013; W. Smyth et al., 2017; W. D. Smyth, 2020).

Furthermore, both numerical simulations and observational data suggest that shear-driven mixing events are not only well-characterised by being (close to) marginal linear stability, but also tend to be in another 'critical' or marginal state where the length scale ratio $R_{OT} \sim 1$ (e.g. Dillon (1982); Ivey and Imberger (1991b)). R_{OT} is defined as the ratio of the Ozmidov length scale L_O to the Thorpe scale L_T

$$R_{OT} := \frac{L_O}{L_T};\ L_O := \left(\frac{\epsilon}{N^3}\right)^{1/2}, \tag{2}$$

where ϵ is the turbulent kinetic energy (density) dissipation rate, and L_T is the (purely geometric) scale constructed from the root-mean square of the displacements required to sort fluid parcels in a (locally statically unstable) overturning density profile into a monotonic, statically stable distribution. L_O may be interpreted as the largest vertical scale which is essentially unaffected by stratification, while the Thorpe scale may be interpreted as the energetic overturning (and hence turbulence injection) scale.

Mashayek et al. (2021) (hereafter MCA21) argued that this critical matching of length scales is characteristic of an intermediate mixing phase in a turbulent patch's life cycle where L_O is both close to its maximum value during a transient shear-driven mixing event (and so the turbulence is most energetic) and the mixing is most efficient (as the overturning scale $L_T \sim L_O$, and so energy is optimally injected right at the top of the dynamic range of turbulence largely unaffected by the stratification, and so with at least the potential to exhibit an isotropic cascade). Due to the optimally tuned nature of this phase of the flow evolution, they referred to it as the 'Goldilocks' mixing phase. One of the two primary goals of this manuscript is to investigate whether there is a connection between the marginal stability paradigm based on Ri and the Goldilocks

paradigm of MCA21 based on R_{OT}, i.e. is it possible to identify this emergent optimal state conceptually with some marginally stable state of the flow. It is our second primary goal herein to test whether in complex, realistic flows, specifically those not characterized by directly forced shear instability (as discussed in W. D. Smyth (2020)), a generalised marginal stability/SOC paradigm for shear-driven overturning mixing is of value for describing significant mixing events.

To investigate the above-mentioned two goals, namely (I) the potential connection between shear-driven marginal stability and the R_{OT}-based Goldilocks mixing paradigm, and (II) the relevance of (generalized) marginal stability to dynamically complex oceanic turbulence zones, we consider three regions where it is not immediately clear that shear-driven mixing should be significant. We consider mixing in the Drake Passage, in the Brazil Basin tidal region, and in an abyssal canyon also in the Brazil basin.

Drake Passage

Figure 1 shows one of the most energetic zones in the ocean, the Drake Passage of the Southern Ocean, where strong currents and eddies pass through a narrow constriction and over rough topography. The results are from a snapshot output from an observationally forced and verified ocean model at unprecedentedly high spatial resolution. The model has been shown to reproduce hydrographic structures, mesoscale dynamics, and tracer transports in excellent agreement with observations– see Supplementary Materials for more details. Of particular relevance to this work is the ability of the model to reproduce the small scale mixing in close agreement with observations (see top-right inset in panel *a* of Fig. 1).

Panel *a* shows how an energetic complex full depth internal wave field is excited by flow topography interactions at the bottom and strong westerly winds at the surface. Nonlinear wave-wave and wave-current interactions lead to localized increases in shear, defined as $|S| = \sqrt{(\partial_z U)^2 + (\partial_z V)^2}$ where U and V are the zonal and meridional velocities. S^2, overlain by density contour lines, is shown in panel *b* for a longitude-depth slice of the simulation. The stability criterion marking the emergence (or lack there of) of shear-induced turbulence is a marginal value of the Richardson number, as previously described.

Panel *c* shows Ri, normalized by its marginal value, i.e. the value above which the flow is assumed to be unable to sustain turbulence. Given the high vertical resolution in the model, we set Ri_m to $\frac{1}{3}$, which is close to but actually slightly higher than the canonical linear marginal value of $Ri_L = \frac{1}{4}$. This choice is made because there have been suggestions that existent ambient residual turbulence can bias the stability criterion slightly higher or lower (S. Thorpe et al., 2013; Li et al., 2015; Kaminski & Smyth, 2019). Furthermore, mixing layers often actually re-laminarize at $Ri_m \sim \frac{1}{3}$ (W. D. Smyth & Moum, 2000; Pham & Sarkar, 2010; Mashayek, Caulfield, & Peltier, 2017). Conversely, there is also numerical and observational evidence that appropriate values of Ri_m (i.e. for sustained turbulence) can actually be as low as 0.16 (as reported in (Portwood et al., 2019; Holleman et al., 2016)) through 0.21 (Zhou et al., 2017; van Reeuwijk et al., 2019) to the Miles-Howard criterion inviscid marginal value of $Ri_L = \frac{1}{4}$ (Salehipour et al., 2018; W. D. Smyth et al., 2019; W. D. Smyth, 2020)–the latter provides a collection of observational evidence.

Note that the coarser a model, the higher Ri_m needs to be set to account for the unresolved subgrid-scale turbulence. Indeed, climate models often use $Ri_m = 0.7$. Panel *c* shows that $Ri \approx Ri_m$ at enhanced sheared locations in the interior and along the top margin of the bottom and top boundary layers (the latter hard to see in the figure). Within the boundary layers, the flow is increasingly less stratified, leading to lower values of Ri. Boundary layer turbulence is complex, a topic of extensive active

research, and parameterized heavily in ocean models including ours. Crudely speaking, at the risk of oversimplification, most such parameterizations involve 'shearing' and 'convective' processes within boundary layers, with the former often parameterized based on Ri. In such layers, the flow is strongly unstable to shear instability as opposed to the interior flow which is predominantly marginally stable (S. Thorpe & Liu, 2009).

It is the interior mixing, however, which is the focus of this study. In the interior of our model, mixing is parameterized in terms of Ri using the now classic 'KPP' model of Large et al. (1994):

$$\frac{\kappa}{\kappa_{max}} = \begin{cases} 1, & Ri \leq 0 \\ \left(1 - (Ri/Ri_m)^2\right)^3, & 0 < Ri \leq Ri_m \\ 0, & Ri_m < Ri\,, \end{cases} \tag{3}$$

where $\kappa_{max} = 5 \times 10^{-3}\mathrm{m}^2\mathrm{s}^{-1}$, and $Ri_m = \frac{1}{3}$ as previously mentioned, and κ is the turbulent or eddy diffusivity. As the local Ri approaches Ri_m, the diffusion, and hence the turbulence, is parameterized to decrease, until it is 'switched off' at the chosen input value of Ri_m. When no turbulence is excited by shear in 'quiet' regions, the model's mixing is set to a background value. Since the focus of our study is on a parameterization based around some kind of marginal stability criterion in the ocean interior, we will not discuss the inference of a turbulent diffusivity in the model. However, we'd like to point out that the diffusivity output of the model agrees excellently with observed profiles of microstructure turbulence in the Drake Passage (see top-right corner inset in Fig. 1a; also see Supplementary Materials), implying that the dynamics and the resulting shear distributions are sufficiently resolved in the model for the confident discussion of a stability criterion. Here we will merely use the model's diffusivity output to separate the turbulent regions from the quiet background flow where diffusivity is set to the background κ_b. Thus, employing a model, we can achieve a separation which would not be feasible in the real world.

Figure 1d shows the probability density function (pdf) of Ri in the full 3D domain over turbulent regions and 'quiet' regions. The pdf has a sharp peak at 0.276, marked by the dashed line, which has emerged to occur quite close to the imposed input marginal value of $Ri_m = \frac{1}{3}$. This implies that co-evolution and nonlinear interactions between mesoscale-submesoscale-wave processes have led to a downward cascade of energy that ultimately has led to local increases in shear at sufficiently small scale that the flow has become unstable. Once the top and bottom boundary layers are removed from the distribution (while admitting that shear instability even remains relevant within them), the emergent peak around (input) Ri_m becomes even sharper. It is worth noting that the pdf of Ri closely resembles that of shear and not that of N^2 (not shown), reinforcing the classical argument proposed by (Turner, 1979) that local increases in shear are the drivers of instabilities.

Marginal stability and Goldilocks mixing

Recently MCA21 proposed a unifying parameterization for the turbulent flux coefficient Γ in terms of R_{OT} in the form of

$$\Gamma := \frac{\mathcal{B}}{\epsilon} = A\frac{R_{OT}^{-1}}{1 + R_{OT}^{\frac{1}{3}}},\ \mathcal{B} = \frac{g}{\rho_0}\langle w'\rho'\rangle, \tag{4}$$

where ρ' is the perturbation density, w' is the perturbation velocity (and so $\mathcal{B}$ is the appropriately averaged vertical [specific] density flux, or [negative] buoyancy flux). Assuming that the mixing occurs at Ri_{go} in the range of *marginal* Richardson numbers $1/6 \leq Ri_m \leq \frac{1}{4}$, MCA21 inferred (on physical grounds) that $\frac{2}{5} \leq A \leq \frac{2}{3} \rightarrow \frac{1}{5} \leq \Gamma \leq \frac{1}{3}$, with the canonical value of $\Gamma = \frac{1}{5}$ corresponding to $Ri_m = \frac{1}{6}$, and the upper bound

$\Gamma = \frac{1}{3}$ corresponding to $Ri_m = Ri_L = \frac{1}{4}$ (see Supplementary Materials for further information).

The parameterization (4) tends to $\Gamma \approx A\ R_{OT}^{-4/3}$ in the $R_{OT} >> 1$ limit, which corresponds to decaying turbulence. As reviewed in MCA21, this scaling has been proposed by many authors, dating back to the 'fossil' turbulence arguments of (Gibson, 1987). In the young turbulence limit of $R_{OT} >> 1$, however, Eq. (4) reduces to $\Gamma \approx A\ R_{OT}^{-1}$ which was proposed by MCA21. Moreover, they argued that it is at the intermediate adjustment phase between the two limits which corresponds to optimal mixing, a phase they dubbed 'Goldilocks Mixing' since in parallel with the fairy-tale it exists when there is just the perfect balance between energy available to turbulence from the background shear and the local stratification which induces stratified turbulence, yet suppresses vertical turbulent motions at the same time. Importantly, MCA21 showed that oceanic data of turbulent patches seem to cluster consistently around the Goldilocks limit of $R_{OT} \sim 1$, thus suggesting another emergent marginal phenomenon of flows organizing so that $R_{OT} \sim 1$.

Figure 2-top, reproduced from MCA21, again shows the excellent agreement between the Goldilocks parameterization (4) with six oceanic datasets comprising a total of ∼50,000 turbulent patches excited by different turbulence processes at different geographical and oceanic depths (see Supplementary Materials for a brief description of the data and MCA21 for comparisons for individual datasets). Interestingly, inferring A from regressing (4) to the diverse collated dataset yields A=0.68∼2/3 which corresponds to $Ri_{go} = Ri_m = Ri_L = \frac{1}{4}$. This is a clear hint that *marginally stable* shear instability is broadly relevant to interior ocean mixing. It also highlights the power of (4) in that it is entirely based on physical grounds, even up to the coefficient A (i.e. assuming that maximally efficient or optimal mixing occurs close to the marginal Richardson number at which shear turbulence can be maintained), and agrees well with data.

The use of appropriate definitions of a buoyancy Reynolds number Re_b, where

$$Re_b \equiv \frac{\epsilon}{\nu N^2} \equiv \left(\frac{L_O}{L_K}\right)^{4/3},\ L_K \equiv \left(\frac{\nu^3}{\epsilon}\right)^{1/4}, \tag{5}$$

where ν is the kinematic viscosity, and L_K is the Kolmogorov microscale, and/or a Richardson number Ri to quantify the flux coefficient is relatively well established (Peltier & Caulfield, 2003; Ivey et al., 2008; Gregg et al., 2018; Caulfield, 2021). However, various datasets do not overlap when mapped onto these parameters (Bouffard & Boegman, 2013; Mashayek, Salehipour, et al., 2017; Monismith et al., 2018). To highlight this tendency in the datasets employed in this article, Fig. 2-bottom plots the same dataset as in the top panel but against Re_b. Put bluntly, the data are all over the place, and so some further analysis is required to resolve the scatter.

On dimensional grounds, more than one nondimensional parameter is required to quantify mixing (Ivey & Imberger, 1991a; Shih et al., 2005; Mashayek & Peltier, 2011, 2013; Mater & Venayagamoorthy, 2014). (Re_b, Ri) is perhaps an obvious pair of parameters on which Γ might reasonably be assumed to depend particularly for shear-driven stratified mixing, although other pairs have been proposed before (Ivey & Imberger, 1991a; Mater & Venayagamoorthy, 2014). Through the lens of the three stage 'Goldilocks mixing' life cycle a parameterization based on Re_b and Ri may be proposed in such a way that demonstrates at least reasonable agreement with the data. There is substantial empirical evidence that for sufficiently large Re_b, $\Gamma \propto Re_b^{-1/2}$ (Ivey et al., 2008; Bouffard & Boegman, 2013; Mashayek, Salehipour, et al., 2017; Monismith et al., 2018). There is also some evidence from experimental and numerical data (see review in Bouffard and Boegman (2013); also see Mashayek, Salehipour, et al. (2017)) that for smaller Re_b, $\Gamma \propto Re_b^{1/2}$. Finally, there is also substantial evidence for $\Gamma \propto Ri$ in not strongly stratified flows particularly when Ri is identified with the inverse square of

an appropriate Froude number $Fr \equiv U/NL$ where U and L are characteristic velocity and length scales (Shih et al., 2005; Wells et al., 2010; Lozovatsky & Fernando, 2013; Salehipour & Peltier, 2015; Zhou et al., 2017; Maffioli et al., 2016). Combining these various observations into a simple empirical relation consistent with Eq. (4), we obtain (see Supplementary Materials)

$$\Gamma = A \frac{Re_b^{*1/2} Ri^*}{1 + Re_b^*}, \tag{6}$$

where

$$Re_b^* = \frac{Re_b}{Re_{bm}}, \qquad Ri^* = \frac{Ri}{Ri_m}, \tag{7}$$

where Ri_m and Re_m are the values of Ri and Re_b where the Goldilocks mixing phase occurs, i.e. where $R_{OT} \sim 1$. This generalizes (to include Re_b) the observation that the Goldilocks mixing phase appears to occur effectively at a marginal or critical value of $Ri_{go} \simeq Ri_m$.

By normalizing Re_b and Ri with their values evaluated at $R_{OT} \sim 1$, Eq. (6) may be interpreted analogously to Eq. (4) as representing two limits of the young/growing turbulence ($Re_b^* \ll 1$) and fossilizing/decaying turbulence ($Re_b^* \gg 1$), smoothly connected at $Re_b^* \approx Ri_* \approx R_{OT} \sim 1$, i.e. at the special (in some sense marginal) values of buoyancy Reynolds number and Richardson number at which $R_{OT} \sim 1$, within the Goldilocks mixing phase. This has two significant implications.

First, it explains (at least partially) the shift of the peak of the curves in Fig. 2-bottom (with variations in Ri explaining the rest); the mere existence of peaks in those curves implies the relevance of the idea of a flow case-sensitive critical or marginal Re_b. Second, it implies that the concept of marginal stability based purely on a special value of $Ri = Ri_L$ associated with the onset of linear shear instability is only a part of the picture and an appropriate two-parameter generalization is essential as implied by the observed peaks of distributions varying with both Ri and Re_b. For example, W. D. Smyth (2020) subsampled the most intense turbulent patches (i.e. focused on a particular narrower range of Re_b) to show that those patches appeared to be in an apparently linearly marginal state with $Ri_m \sim Ri_L = \frac{1}{4}$.

Using the hypothesis that turbulent flows organize and mix with $\mathrm{R}_{OT} \sim 1$, on the other hand, seems to be a more natural generalized critical or 'marginal stability' criterion, at least with respect to parameterizing the turbulent flux coefficient Γ. Furthermore, while Ri and Re_b vary over a few to several orders of magnitude, 80% of data in Fig. 2 lie within a factor of 3 of $R_{OT} = 1$, implying that expressing and quantifying mixing in terms of values of R_{OT} is much more suitable.

Direct application to ocean data

We now show that Eq. (4) and Eq. (6) appear to agree reasonably well when applied to two oceanic datasets that include all the parameters involved in the two formulations. Two of the datasets used in Fig. 2 were from the Brazil Basin Tracer Release Experiment (BBTRE), and the Dynamics of Mid-Ocean Ridge Experiment (DoMORE). The former sampled turbulence induced by internal tide shear in the deep Brazil Basin over the mid-Atlantic ridge (Polzin et al., 1997) while the latter sampled turbulence over a sill on a canyon floor also in the Brazil Basin (Clément et al., 2017). So, while for BBTRE it is expected that nonlinear wave-wave interactions will downscale energy to small scales where shear instabilities can ultimately kick in (e.g. see (Nikurashin & Legg, 2011)), the flow is expected to be somewhat hydraulically controlled for DoMORE with at least part of the sampled turbulence corresponding to boundary layer turbulence, somewhat similar to the deepest canyons in Fig. 1c. The two datasets were recently analysed by Ijichi et al. (2020) where they identified turbulence patches and calculated their corresponding L_O, L_T, and Ri values. This is convenient for our

purposes as most often explicit shear measurements co-located with profiles of density and ϵ are lacking.

The first test is whether the connection we made between the Ri_L-based linear marginal instability criterion and the proposed generalized stability criterion of R_{OT}-based Goldilocks mixing holds, based on the heuristic equivalency of Eq. (4) and Eq. (6). We start by inferring appropriate values of Ri_m and Re_{bm} through appropriately averaging the observational values of these quantities associated with observations where $R_{OT} \sim 1$. We then equate the value of Γ constructed directly from the observations of R_{OT} using Eq. (4) with the value of Γ given by Eq. (6). In Eq. (6), we input measured Re_b, and the inferred values of Ri_m and Re_{bm} to obtain a parameterization prediction for Ri_{param}. Figure 3a,b show this Ri_{param}, plotted against the directly measured Ri. The agreement is impressive for the peak of both pdfs. For BBTRE, the agreement seems to also hold nicely over the entire range of Ri, consistent with the hypothesis that the ocean interior is close to marginally stable and turbulence bursts are excited by localized increases in shear (thereby a local drop in Ri). For DoMORE, on the other hand, the data consists of patches both within and outside of the bottom boundary layer. Thus, the range of Ri extends from close to $Ri_L = \frac{1}{4}$ to much smaller values compared to BBTRE (somewhat similar to Fig. 2b,c). Richardson numbers inferred from equating the two expressions for Γ, Eq. (4) and (6), tend to over-predict the low end of Ri in Fig. 3b as Eqs. (4), (6) are meant to only apply to interior mixing, 'sufficiently' far from boundary layer turbulence so that shear layers are 'free'. According to Fig. 1c, the upper end of the bottom boundary layer marks the limits of the relevance of (4), (6) and coincidentally is where they are quite actively relevant as that interface is rife with shear-driven turbulence (similar to mixing at the base of the surface ocean mixed-layer).

Figure 3c,d further illustrate the correspondence between the generalized marginal stability criterion based on R_{OT} and a more conventional marginal stability criterion based purely on Ri_m. Panel c shows that for turbulent patches sampled during BBTRE, the joint probability distribution of Ri and R_{OT} is sharply peaked at $Ri \approx 0.2$ and $R_{OT} \approx 1$. In physical terms, most turbulence patches are likely excited through shear instability (hence Ri slightly less than $Ri_L = \frac{1}{4}$) and are in the Goldilocks phase where the APE absorbed from the mean flow is actively energizing the turbulence inertial subrange with L_O as an upper bound. In contrast, panel d shows that for turbulent patches sampled during DoMORE, the distribution of Ri is much more spread, with a peak probability density at a modal Ri value of ~ 0.1. As discussed above, this is due to the near boundary nature of sampling in DoMORE which implies lower stratification and hence lower Ri. The R_{OT} distribution, however, remains tightly bound (similar to BBTRE) with the mode ≈ 1, implying that non-shear-instability-like overturns likely contribute at least to some of the data. Hydraulically induced overturns are some candidates (e.g. MCA21, through analysis of data from Carter et al. (2019), show that the paradigm that $R_{OT} \sim 1$ seems to have relevance to hydraulically induced flow over sills in the abyssal Samoan Passage). Panels c,d, therefore, reinforce our argument that the R_{OT}-based generalized marginal stability criterion (which we have demonstrated can be thought of as having an implicit 2D $Re_b - Ri$ dependence) is more general as compared to one solely based on Ri. A purely Ri-based marginal stability criterion is incomplete without consideration of an appropriate companion Reynolds number and is not directly relevant to non-shear-instability-induced overturns which seem to abound in boundary layers.

Figures 3e,f further emphasizes the points made above by showing how the modal values of the distributions of Ri, R_{OT} and their joint distribution vary for patches with quantiles of ε. For BBTRE, for all the data (weakly turbulent and strongly turulent patches) the marginal shear instability criterion based on a marginal value Ri_m appears to hold while $R_{OT} \sim 1$ for most patches except for the top quantile

of ε for which the modal value is $R_{OT} \sim 2$. This is perhaps unsurprising since the most energetic phase of turbulence often occurs simultaneously with or shortly after turbulence has grown rapidly (and so L_O is maximal) at the cost of the conversion of some of the stored APE in the overturn (and so L_T has fallen from its maximum). For DoMORE, as discussed above, the patches closer to the boundary correspond to relatively low stratification and Ri while those further away and in the interior are still likely prone to shear instability (noting that shear instabilities can still be relevant in deep canyons and flows over sills (e.g. Alford et al., 2013)). For all the quantiles of data in DoMORE, $R_{OT} \sim 1$, highlighting again the more general applicability of our proposed generalized marginal stability criterion based on R_{OT}.

Discussion

We have investigated the relevance of a criterion based on the concept of marginally stable shear instabilities and found that in the ocean interior such a criterion is relevant even in dynamically complex regions. In such regions, energy downscales from mesoscales and submesoscale dynamics, or from the internal wave field (e.g. induced by tides) to scales sufficiently small that localized shear can induce small scale shear instability and mixing. Within the boundary layers, using a Ri-based criterion alone is not so successful.

We have shown that a generalized marginal stability criterion based on assuming that the flow adjusts towards $R_{OT} \sim 1$ holds in the interior and seemingly also within the boundary layers. We have demonstrated that the R_{OT} marginal stability criterion can be related to an alternative criterion, which explicitly depends jointly on Ri and Re_b. We have argued that a collection of oceanic datasets show that each field experiment (or turbulence region) has its own flow case-sensitive generalized marginal stability criterion with respect to the particular marginal values of Re_{bm} and Ri_m, whereas the $R_{OT} \sim 1$ criterion holds more universally, and hence more usefully. Our finding sheds light on the seeming significant discrepancy between parameterization of ocean mixing based on Re_b alone and puts bounds on the relevance of the conventional marginal shear instability criterion based purely on linear stability arguments that $Ri_m \simeq Ri_L = \frac{1}{4}$.

The parameterization proposed in MCA21 for the flux coefficient Γ, as reviewed in Fig. 2a, together with the ability of the generalized marginal stability criterion based around $R_{OT} \sim 1$ to cross over from interior turbulence to boundary layer dynamics, have the potential to be very useful. In tandem, they allow unified consideration of several different mixing regimes. For example, it is possible to consider: (i) weak mixing in the ocean interior far from the boundaries (where there is less energy available to turbulence and the stratification is relatively strong); (ii) energetic efficient mixing in the vicinity of the boundary between interior dynamics and boundary layers (where the 'right' balance of shear and stratification leads to the most efficient mixing, dubbed as 'Goldilocks Mixing' by MCA21); and (iii) weakly mixing regions deep within boundary layers (where while energy is available, stratification is weak and hence there is less to mix).

There has been a recent paradigm shift in our understanding of the role of deep ocean turbulence in the global ocean overturning circulation, thereby in the climate system. The new paradigm suggests that the turbulence in the ocean interior above rough topography can lead to densification and downwelling of water masses, while boundary layer turbulence is primarily responsible for lightening and upwelling of the dense waters that form as such plus the dense waters that form at high latitude and sink to the deep ocean (Mashayek et al., 2015; de Lavergne et al., 2016b; Ferrari et al., 2016; de Lavergne et al., 2017). The transition from interior downwelling to boundary upwelling is marked by a change in the sign of the vertical gradient of the effective

flux of buoyancy, approximated as the multiplication of the local flux coefficient and the local rate of dissipation of kinetic energy. Thus, accurate quantification of the flux coefficient is key to an accurate calculation of the deep branch of ocean circulation. Before the work presented here, parameterizations of small scale mixing based on Ri and/or Re_b have so far been incapable of fully capturing the subtlety of transitioning from interior to boundary mixing (de Lavergne et al., 2016a; Mashayek, Salehipour, et al., 2017; Cimoli et al., 2019).

References

Alford, M. H. (2020). Global calculations of local and remote near-inertial-wave dissipation. *Journal of Physical Oceanography*, *50*(11), 3157–3164.

Alford, M. H., Girton, J. B., Voet, G., Carter, G. S., Mickett, J. B., & Klymak, J. M. (2013). Turbulent mixing and hydraulic control of abyssal water in the Samoan Passage. *Geophysical Research Letters*, *40*(17), 4668–4674.

Bak, P., Tang, C., & K, W. (1987). Self-organized criticality - an explanation of $1/f$ noise. *Phys. Rev. Lett.*, *59*, 381-384.

Bouffard, D., & Boegman, L. (2013). A diapycnal diffusivity model for stratified environmental flows. *Dynamics of Atmospheres and Oceans*.

Carter, G. S., Voet, G., Alford, M. H., Girton, J. B., Mickett, J. B., Klymak, J. M., ... Tan, S. (2019). *A spatial geography of abyssal turbulent mixing in the samoan passage* (Vol. 32; Tech. Rep. No. 4). doi: 10.5670/oceanog.2019.425

Caulfield, C. P. (2021, 1). Layering, Instabilities, and Mixing in Turbulent Stratified Flows. *Annual Review of Fluid Mechanics*, *53*(1), 113–145. Retrieved from `https://doi.org/10.1146/annurev-fluid-042320-` doi: 10.1146/annurev-fluid-042320-100458

Cimoli, L., Caulfield, C. P., Johnson, H. L., Marshall, D. P., Mashayek, A., Naveira Garabato, A. C., & Vic, C. (2019, 12). Sensitivity of Deep Ocean Mixing to Local Internal Tide Breaking and Mixing Efficiency. *Geophysical Research Letters*, *46*(24), 14622–14633. Retrieved from `https://onlinelibrary.wiley.com/doi/abs/10.1029/2019GL085056` doi: 10.1029/2019GL085056

Clément, L., Thurnherr, A. M., & St. Laurent, L. C. (2017). Turbulent mixing in a deep fracture zone on the Mid-Atlantic Ridge. *Journal of Physical Oceanography*, *47*(8), 1873–1896. doi: 10.1175/JPO-D-16-0264.1

de Lavergne, C., Madec, G., Le Sommer, J., Nurser, A. J. G., & Naveira Garabato, A. C. (2016a, 2). The Impact of a Variable Mixing Efficiency on the Abyssal Overturning. *Journal of Physical Oceanography*, *46*(2), 663–681. Retrieved from `http://journals.ametsoc.org/doi/10.1175/JPO-D-14-0259.1` doi: 10.1175/JPO-D-14-0259.1

de Lavergne, C., Madec, G., Le Sommer, J., Nurser, A. J. G., & Naveira Garabato, A. C. (2016b, 2). On the Consumption of Antarctic Bottom Water in the Abyssal Ocean. *Journal of Physical Oceanography*, *46*(2), 635–661. Retrieved from `http://journals.ametsoc.org/doi/10.1175/JPO-D-14-0201.1` doi: 10.1175/JPO-D-14-0201.1

de Lavergne, C., Madec, G., Roquet, F., Holmes, R. M., & McDougall, T. J. (2017, 11). Abyssal ocean overturning shaped by seafloor distribution. *Nature*, *551*(7679), 181–186. Retrieved from `http://www.nature.com/articles/nature24472` doi: 10.1038/nature24472

Dillon, T. M. (1982). Vertical overturns: A comparison of Thorpe and Ozmidov length scales. *Journal of Geophysical Research*, *87*(C12), 9601. doi: 10.1029/jc087ic12p09601

Ferrari, R., Mashayek, A., McDougall, T. J., Campin, J.-M., & Nikurashin, M. (2016). Turning Ocean Mixing Upside Down. *Journal of Physical Oceanography*. doi: 10.1175/jpo-d-15-0244.1

Garrett, C., & Kunze, E. (2007). Internal tide generation in the deep ocean. *Annu. Rev. Fluid Mech.*, *39*, 57–87.

Geyer, W. R., Lavery, A. C., Scully, M. E., & Trowbridge, J. H. (2010). Mixing by shear instability at high {Reynolds} number. *Geophys. Res. Lett.*, *37*, L22607.

Gibson, C. H. (1987). Fossil turbulence and intermittency in sampling oceanic mixing processes. *Journal of Geophysical Research: Oceans (1978–2012)*, *92*(C5), 5383–5404.

Gregg, M., D'Asaro, E., Riley, J., & Kunze, E. (2018, 1). Mixing Efficiency in the Ocean. *Annual Review of Marine Science*, *10*(1), 443–473. Retrieved from `http://www.annualreviews.org/doi/10.1146/annurev-marine-121916-063643` doi: 10.1146/annurev-marine-121916-063643

Holleman, R., Geyer, W., & Ralston, D. (2016). Stratified turbulence and mixing efficiency in a salt wedge estuary. *Journal of Physical Oceanography*, *46*(6), 1769–1783.

Howard. (1961). Note on a paper of John W. Miles. *J. Fluid Mech.*, *10*, 509–512.

Ijichi, T., St. Laurent, L., Polzin, K. L., & Toole, J. M. (2020). How Variable Is Mixing Efficiency in the Abyss? *Geophysical Research Letters*, *47*(7), 1–9. doi: 10.1029/2019GL086813

Ivey, G. N., & Imberger, J. (1991a). On the nature of turbulence in a stratified fluid. Part I: The energetics of mixing. *J. PHYSICAL OCEANOGRAPHY*, *21*(5 May), 650–658.

Ivey, G. N., & Imberger, J. (1991b, 5). On the nature of turbulence in a stratified fluid. Part I: The energetics of mixing. *J. PHYSICAL OCEANOGRAPHY*, *21*(5 May), 650–658. doi: 10.1175/1520-0485(1991)021⟨0650:otnoti⟩2.0.co;2

Ivey, G. N., Winters, K. B., & Koseff, J. R. (2008). Density stratification, turbulence, but how much mixing? *Annu. Rev. Fluid Mech.*, *40*, 169–184.

Kaminski, A. K., & Smyth, W. D. (2019). Stratified shear instability in a field of pre-existing turbulence. *Journal of Fluid Mechanics*, *862*, 639–658. doi: 10.1017/jfm.2018.973

Large, W. G., McWilliams, J. C., & Doney, S. C. (1994). Oceanic vertical mixing: A review and a model with a nonlocal boundary layer parameterization. *Reviews of Geophysics*, *32*(4), 363–403.

Legg, S. (2021). Mixing by oceanic lee waves. *Annual Review of Fluid Mechanics*, *53*.

Li, L., Smyth, W., & Thorpe, S. (2015). Destabilization of a stratified shear layer by ambient turbulence. *Journal of Fluid Mechanics*, *771*, 1–15.

Lozovatsky, I. D., & Fernando, H. J. S. (2013). Mixing efficiency in natural flows. *Philosophical Transactions of the Royal Society A: Mathematical, Physical and Engineering Sciences*, *371*(1982).

Maffioli, A., Brethouwer, G., & Lindborg, E. (2016). Mixing efficiency in stratified turbulence. *J. Fluid Mech*, *794*, R3. Retrieved from `https://doi.org/10.1017/jfm.2016.206` doi: 10.1017/jfm.2016.206

Mashayek, A., Caulfield, C. P., & Alford, M. H. (2021). Goldilocks mixing in shear-induced ocean turbulence. *https://arxiv.org/abs/2108.05284*(Accepted for publication in the Journal of Fluid Mechanics).

Mashayek, A., Caulfield, C. P., & Peltier, W. R. (2017). Role of overturns in optimal mixing in stratified mixing layers. *Journal of Fluid Mechanics*, *826*, 522–552.

Mashayek, A., Ferrari, R., Merrifield, S., Ledwell, J. R., St Laurent, L., & Garabato, A. N. (2017). Topographic enhancement of vertical turbulent mixing in the Southern Ocean. *Nature communications*, *8*, 14197.

Mashayek, A., Ferrari, R., Nikurashin, M., & Peltier, W. R. (2015). Influence of Enhanced Abyssal Diapycnal Mixing on Stratification and the Ocean Overturning Circulation. *J. Phys. Oceanogr.*, *45*(10), 2580–2597.

Mashayek, A., & Peltier, W. R. (2011). Turbulence transition in stratified atmospheric and oceanic shear flows: Reynolds and Prandtl number controls upon

the mechanism. *Geophysical Research Letters*, *38*, L16612, 5 PP.

Mashayek, A., & Peltier, W. R. (2013). Shear-induced mixing in geophysical flows: does the route to turbulence matter to its efficiency? *Journal of Fluid Mechanics*, *725*, 216–261.

Mashayek, A., Salehipour, H., Bouffard, D., Caulfield, C. P., Ferrari, R., Nikurashin, M., ... Smyth, W. D. (2017). Efficiency of turbulent mixing in the abyssal ocean circulation. *Geophysical Research Letters*, *44*(12), 6296–6306.

Mater, B. D., & Venayagamoorthy, S. K. (2014). A unifying framework for parameterizing stably stratified shear-flow turbulence. *Physics of Fluids (1994-present)*, *26*(3), 36601.

Miles, J. W. (1961). On the stability of heterogeneous shear flows. *J. Fluid Mech.*, *10*, 496–508.

Monismith, S. G., Koseff, J. R., & White, B. L. (2018). Mixing efficiency in the presence of stratification: When is it constant? *Geophysical Research Letters*.

Nikurashin, M., & Ferrari, R. (2013). Overturning Circulation Driven by Breaking Internal Waves. *Journal of Physical Oceanography*, DOI: 10.1002/grl.50542.

Nikurashin, M., & Legg, S. (2011). A mechanism for local dissipation of internal tides generated at rough topography. *J. Phys. Oceanogr.*, *41*, 378–395.

Peltier, W. R., & Caulfield, C. P. (2003). Mixing efficiency in stratified shear flows. *Annual Rev. Fluid Mech.*, *35*, 135–167.

Pham, H. T., & Sarkar, S. (2010). Transport and mixing of density in a continuously stratified shear layer. *Journal of Turbulence*, *24*, 1–23.

Polzin, K. L., Toole, J. M., Ledwell, J. R., & Schmitt, R. W. (1997). Spatial variability of turbulent mixing in the abyssal ocean. *Science*, *276*(5309), 93–96.

Portwood, G. D., de Bruyn Kops, S. M., & Caulfield, C. P. (2019). Asymptotic dynamics of high dynamic range stratified turbulence. *Phys. Rev. Lett.*, *122*, 194504.

Salehipour, H., & Peltier, W. R. (2015). Diapycnal diffusivity, turbulent Prandtl number and mixing efficiency in Boussinesq stratified turbulence. *J. Fluid Mech.*, *775*, 464–500.

Salehipour, H., Peltier, W. R., & Caulfield, C. P. (2018). Self-organised criticality of turbulence in strongly stratified mixing layers. *J. Fluid Mech.*, *856*, 228–256.

Shih, L. H., Koseff, J. R., Ivey, G. N., & Ferziger, J. H. (2005). Parameterization of turbulent fluxes and scales using homogeneous sheared stably stratified turbulence simulations. *J. Fluid Mech.*, *525*, 193–214.

Smyth, W., Pham, H., Moum, J., & Sarkar, S. (2017). Pulsating turbulence in a marginally unstable stratified shear flow. *Journal of Fluid Mechanics*, *822*, 327–341.

Smyth, W. D. (2020). Marginal instability and the efficiency of ocean mixing. *J. Phys. Oceanogr.*, *50*, 2141–2150.

Smyth, W. D., & Moum, J. N. (2000). Length scales of turbulence in stably stratified mixing layers. *Physics of Fluids*, *12*, 1327.

Smyth, W. D., & Moum, J. N. (2013). Marginal instability and deep cycle turbulence in the eastern equatorial Pacific Ocean. *Geophys. Res. Lett.*, *40*, 6181-6185.

Smyth, W. D., Nash, J. D., & Moum, J. N. (2019). Self-organized criticality in geophysical turbulence. *Sci. Reports*, *9*, 3747.

Talley, L. D., Feely, R. A., Sloyan, B. M., Wanninkhof, R., Baringer, M. O., Bullister, J. L., ... Zhang, J. Z. (2016, 1). Changes in Ocean Heat, Carbon Content, and Ventilation: A Review of the First Decade of GO-SHIP Global Repeat Hydrography. *Annual Review of Marine Science*, *8*, 185–215. Retrieved from `www.go-ship.org` doi: 10.1146/annurev-marine-052915-100829

Thorpe, S., & Liu, Z. (2009). Marginal instability? *Journal of physical oceanography*, *39*(9), 2373–2381.

Thorpe, S., Smyth, W., & Li, L. (2013). The effect of small viscosity and dif-

fusivity on the marginal stability of stably stratified shear flows. *J. Fluid Mech.,(submitted)*.

Thorpe, S. A. (2005). The turbulent ocean. *Cambridge University Press*.

Thorpe, S. A., & Liu, Z. (2009). Marginal instability? *J. Phys. Oceanogr.*, *39*, 2373–2381.

Turner, S. (1979). *Buoyancy effects in fluids*. Cambridge University Press.

van Reeuwijk, M., Holzner, M., & Caulfield, C. P. (2019). Mixing and entrainment are suppressed in inclined gravity currents. *J. Fluid Mech.*, *873*, 786?815.

van Haren, H., & Gostiaux, L. (2010). A deep-ocean Kelvin-Helmholtz billow train. *Geophys. Res. Lett.*, *37*, 1-5.

Wells, M., Cenedese, C., & Caulfield, C. P. (2010). The relationship between flux coefficient $Γ$ and entrainment ratio E in density currents. *J. Phys. Oceanogr.*, *40*, 2713–2727.

Woods, J. D. (1968). Wave-induced shear instability in the summer thermocline. *J. Fluid Mech.*, *32*, 791–800.

Wunsch, C., & Ferrari, R. (2004). Vertical mixing, energy, and the general circulation of the oceans. *Annu. Rev. Fluid Mech.*, *36*, 281–314.

Zhou, Q., Taylor, J. R., & Caulfield, C. P. (2017). Self-similar mixing in stratified plane Couette flow for varying Prandtl number. *J. Fluid Mech.*, *820*, 86–120.

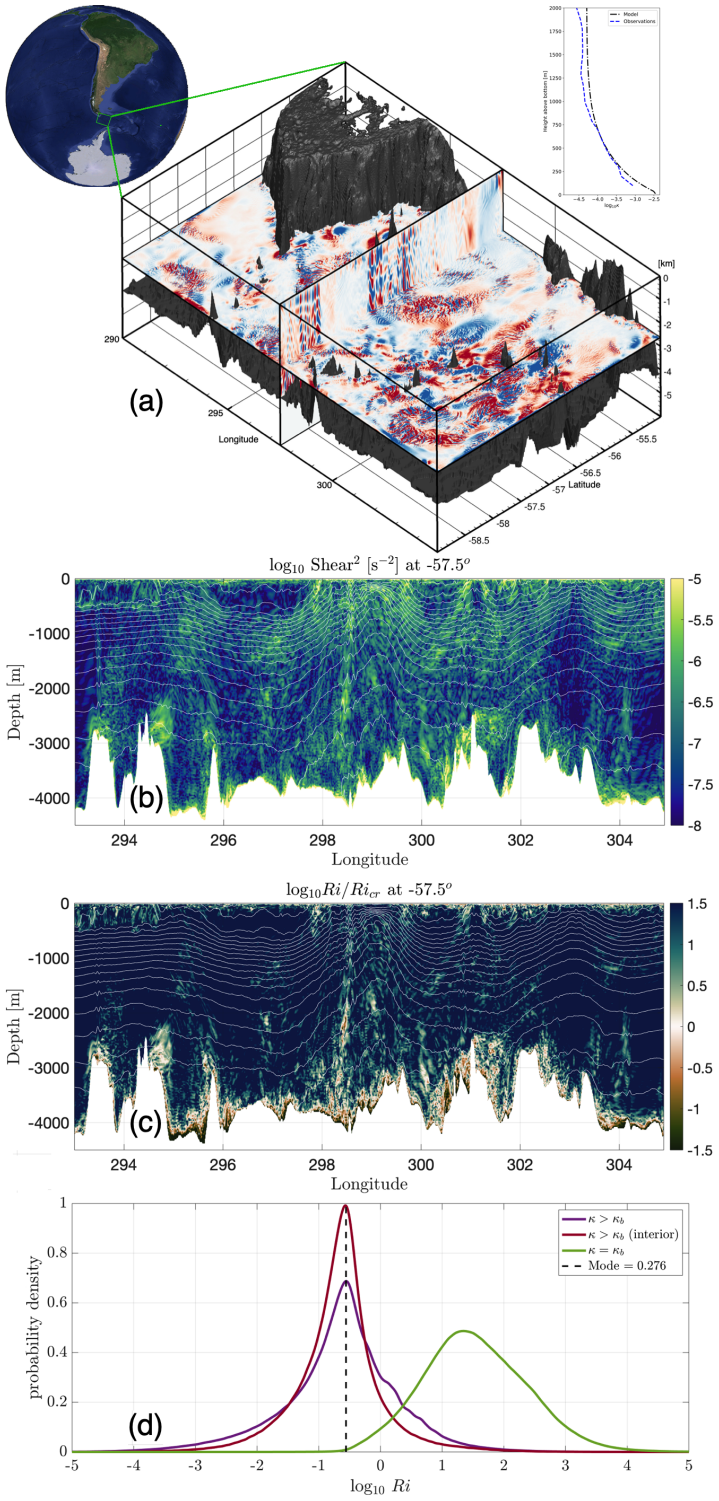

Figure 1. (a) A sector of the Southern Ocean in which strong westerly winds at the surface and interaction of Antarctic Circumpolar Current system (ACC; illustrated by the black lines) with rough topography create an energetic internal wave field. From an observationally forced and tuned high resolution numerical simulation(Mashayek, Ferrari, et al., 2017). The top-right inset shows the model model diffusivity, κ, compared with microstructure observations from DIMES. (b) A longitude-depth slice of squared shear (i.e. vertical gradient of horizontal velocity) superimposed by density layers (white lines). (c) Richardson number normalized by the marginal value of 0.33) used in the model. (d) Probability density function of Richardson number for turbulent regions for the full 3D domain, for the full domain excluding the top and bottom 200m, and for the non-turbulent background regions. Turbulent regions are where turbulence level is above the model background value of $\kappa_b = 5 \times 10^{-5}$ m^{2}s^{-1}. The top and bottom 200m are excluded in one case to exclude mixed layer and bottom boundary layer where other parameterized processes, in addition to shear instability, can create mixing in the model.

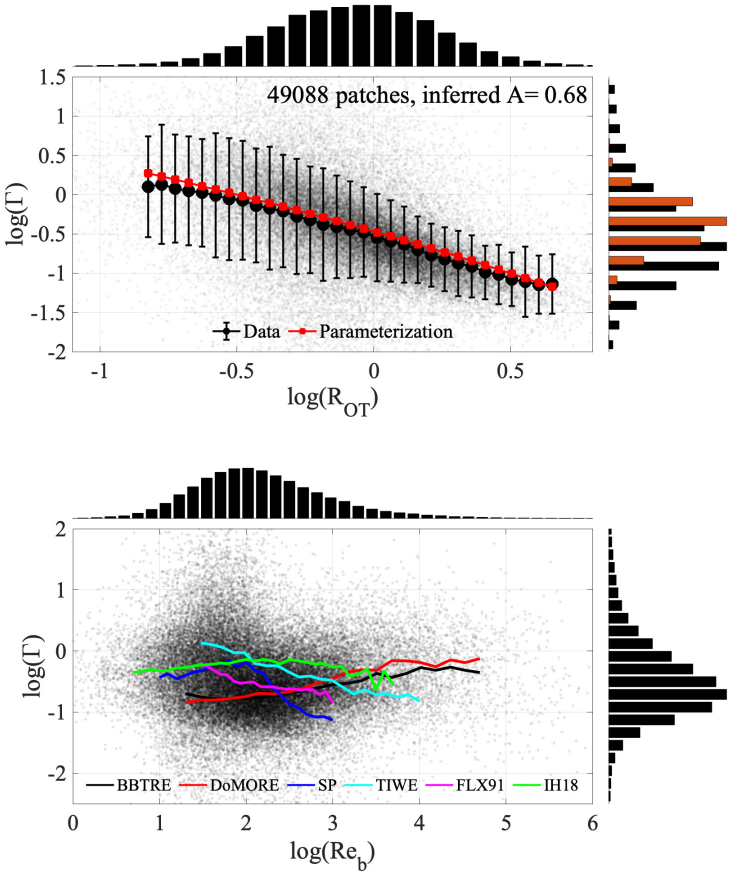

Figure 2. Distribution of the flux coefficient as a function of $R_{OT} = L_O/L_T$ (top) and $Re_b = \epsilon/(\nu N^2)$ (bottom) from ∼50,000 turbulent patches from a total of six oceanic experiments covering a wide range of depth, geographic locations, and turbulence generation processes; see Supplementary Information for a description of the datasets. The original patch data is shown in small blue dots (with their histograms shown along the right and top axes) and the experiment-binned/mean distributions are shown in thick lines with large symbols in the top panel and with thick lines in the bottom panel. Both panels are reproduced from Mashayek et al. (2021) where details of the datasets may be found.

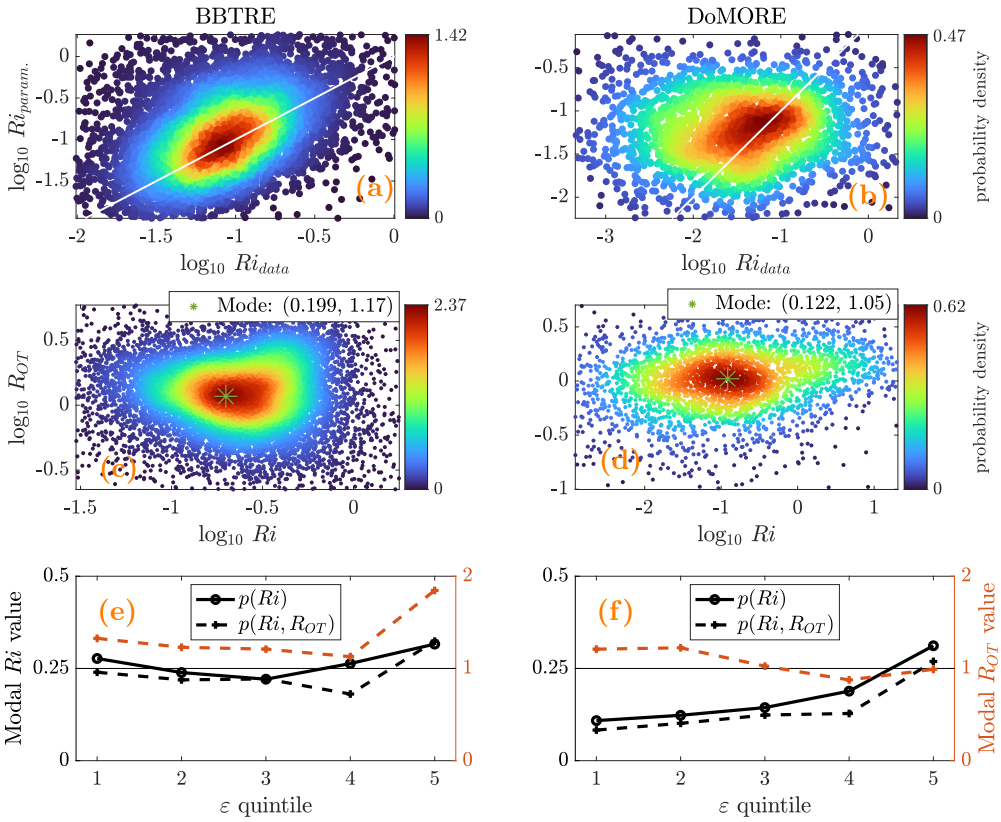

Figure 3. Joint probability distribution for Ri from data and inferred from parameterization (6) as described in the text for BBTRE (a) and DoMORE (b). White line corresponds to $Ri_{data} = Ri_{param.}$. Scatterpoint color indicates local probability density. (c,d) Joint probability distribution of Ri and R_{OT} for BBTRE and DoMORE. Green cross indicates estimated mode of probability distribution. The modal values are shown in the legend (not in log).(e,f) Modal values for probability distribution of Ri alone and for joint distribution of Ri and R_{OT} for different ε quintiles of patches in BBTRE and DoMORE.

Supplementary Materials: A generalized marginal stability criterion for shear-induced ocean interior diapycnal turbulent mixing

A. Mashayek[1*], L. E. Baker[1], B.B. Cael[2], and C. P. Caulfield[3]

[1]Imperial College London
[2]National Oceanography Centre Southampton
[3]University of Cambridge

Model setup and verification

We use recent high resolution, nested simulations of the Drake Passage region, performed using the hydrostatic configuration of the Massachusetts Institute of Technology general circulation model (MITgcm, Marshall et al., 1997). The horizontal resolution is 0.01°, and there are 225 vertical levels, with 10m resolution at the surface decreasing to 25m at 4500m. For details of a similar model setup, see Mashayek, Ferrari, et al. (2017). The model shown here differs in improved vertical resolution, which allows better resolution of the internal wave field. The vertical diffusivity and viscosity have background values of 5×10^{-5} m^{2}s^{-1}, and are enhanced by the Richardson number based K-Profile parametrization (KPP, Large et al., 1994), with a critical Richardson number for shear instability set at 0.33.

The domain is nested within a larger Southern Ocean 'parent' patch (Tulloch et al., 2014), which is itself restored at the open boundaries to velocities, temperature and salinity from the Ocean Comprehensive Atlas (OCCA), an 18-month-long ocean state estimate (Forget, 2010). Tulloch et al. (2014) showed that the stratification and velocities in their model were consistent with data from the World Ocean Circulation Experiment (WOCE). Tangential and normal velocities from the 'parent' patch are applied as open boundary conditions to the Drake Passage domain, and temperature and salinity are restored to the 'parent' model within a 1° sponge layer.

Mashayek, Ferrari, et al. (2017) demonstrate that the model reproduces tracer diffusivity in the region, consistent with observations from the diapycnal and isopycnal mixing experiment in the Southern Ocean (DIMES). Figure 1a shows that the more recent (higher vertical resolution) simulations used here also show skill in reproducing observed microstructure diffusivity from DIMES using the KPP parametrization for diffusivity.

Ocean data

The datasets used in Fig. 2 are briefly discussed here. More details are provided in MCA21 from which Fig. 2 is reproduced. The six oceanic datasets employed for the purposes of analyses in this article are the same as those employed by MCA21. Here we provide a brief description and refer to MCA21 for a more comprehensive discussion. The Tropical Instability Wave Experiment (TIWE) dataset includes turbulent patches sampled at the equator at 140°W in the shear-dominated upper-equatorial thermocline, between 60m and 200m depths, spanning both the upper and lower flanks of the Pacific Equatorial Undercurrent (Lien et al., 1995; Smyth et al., 2001). The FLUX STAT (FLX91) experiment sampled turbulence at the thermocline (∼350-500m depth), in

*The last three authors are listed in alphabetical order.

Corresponding author: Ali Mashayek, mashayek@imperial.ac.uk

part generated through shear arising from downward-propagating near-inertial waves, about 1000 km off the coast of northern California (Moum, 1996; Smyth et al., 2001). The IH18 experiment measured full-depth turbulence (up to ∼5300m deep) primarily generated by tidal flow over the Izu-Ogasawara Ridge (western Pacific, south of Japan), a prominent generation site of the semidiurnal internal tide that spans the critical latitude of 28.88N for parametric subharmonic instability (Ijichi & Hibiya, 2018). The Samoan Passage data are measurements of abyssal turbulence generated by hydraulically-controlled flow over sills in the depth range 4500-5500m in the Samoan Passage, an important topographic constriction in the deep limb of the Pacific Meridional Overturning Circulation (Alford et al., 2013; Carter et al., 2019). The BBTRE data are from turbulence induced by internal tide shear in the deep Brazil Basin (∼2500-5000m depth) and were acquired as a part of the original Brazil Basin Tracer Release Expermient (BBTRE; (Polzin et al., 1997)), recently re-analyzed by (Ijichi et al., 2020). Also reanalysed by (Ijichi et al., 2020), we use the data from DoMORE which focused on flow over a sill on a canyon floor in the Brazil Basin (Clément et al., 2017; Ijichi et al., 2020).

Derivation of the R_{OT} and $Re_b - Ri$ based parameterizations

The scaling parameter A in Eq. 4 in the main text can be expressed as

$$A = \frac{2\frac{Ri_{go}}{Pr_t}}{1-\frac{Ri_{go}}{Pr_t}},\ Pr_T := \frac{\nu_T}{\kappa_T}, \tag{1}$$

where Ri_{go} is the Richardson number at which the Goldilocks mixing is assumed to occur, and Pr_T is the turbulent Prandtl number (i.e. the ratio of the eddy diffusivity of momentum to the eddy diffusivity of density). Significantly (see for example (Caulfield, 2021) for more detailed discussion) Pr_T can also be expressed as

$$Pr_T = \frac{N^2}{S^2}\frac{\mathcal{P}}{\mathcal{B}} \equiv \frac{Ri}{Ri_f} \simeq \frac{Ri(1+\Gamma)}{\Gamma}, \tag{2}$$

where $\mathcal{P}$ is the turbulence production and $Ri_f \equiv \mathcal{B}/\mathcal{P}$ is the 'flux Richardson number'. Under several sweeping assumptions, as presented originally by (Osborn, 1980), $\mathcal{P} \simeq \mathcal{B} + \epsilon$, and so $Ri_f \simeq \Gamma/(1+\Gamma)$.

MCA21 argued that the evidence from a range of ocean-relevant turbulent flows suggest that vigorous turbulence with sufficiently small Ri, distinctly characterized by overturns, typically has $Pr_T \simeq 1$ (Zhou et al., 2017; van Reeuwijk et al., 2019; Portwood et al., 2019). The appropriate values of the marginal Richardson number Ri_m, MCA21 argued, range from 0.16 (as reported in Portwood et al. (2019)) through 0.21 (Zhou et al., 2017; van Reeuwijk et al., 2019) to the linearly marginally stable value of $Ri_L = \frac{1}{4}$ (Salehipour et al., 2018; Smyth et al., 2019; Smyth, 2020). The presence of background turbulence in the ocean can also alter the critical value (Smyth et al., 2001; Thorpe et al., 2013; Kaminski & Smyth, 2019). Using $R_{OT} \simeq 1$, $Pr_T \simeq 1$ and the further assumption that the Richardson number Ri_{go} at which the mixing is occuring can be assumed to be in the range of *marginal* Richardson numbers $1/6 \leq Ri_m \leq \frac{1}{4}$ consistent with the previous studies mentioned above, MCA21 inferred from (1) that $\frac{2}{5} \leq A \leq \frac{2}{3} \rightarrow \frac{1}{5} \leq \Gamma \leq \frac{1}{3}$, with the canonical value of $\Gamma = \frac{1}{5}$ corresponding to $Ri_m = \frac{1}{6}$, and the upper bound $\Gamma = \frac{1}{3}$ corresponding to $Ri_m = Ri_L = \frac{1}{4}$.

Combining the various empirical observations reported in the main text into a simple empirical relation, we postulate that

$$\Gamma = \frac{B\ Re_b^{1/2} Ri}{1 + C\ Re_b}, \tag{3}$$

a generalization of the parameterization proposed in Mashayek, Salehipour, et al. (2017), but now with a postulated linear dependence on Ri, consistent with $Pr_T \simeq 1$ and Eq. (2) (see for example (Zhou et al., 2017)).

Heuristically, we can make this expression consistent with Eq. 4 (main text) by rewriting it as

$$\Gamma = A \frac{Re_b^{*\,1/2} Ri^*}{1 + Re_b^*}, \tag{4}$$

when appropriately scaled, as discussed further in the main text.

References

Alford, M. H., Girton, J. B., Voet, G., Carter, G. S., Mickett, J. B., & Klymak, J. M. (2013). Turbulent mixing and hydraulic control of abyssal water in the Samoan Passage. *Geophysical Research Letters*, *40*(17), 4668–4674.

Carter, G. S., Voet, G., Alford, M. H., Girton, J. B., Mickett, J. B., Klymak, J. M., ... Tan, S. (2019). *A spatial geography of abyssal turbulent mixing in the samoan passage* (Vol. 32; Tech. Rep. No. 4). doi: 10.5670/oceanog.2019.425

Caulfield, C. P. (2021, 1). Layering, Instabilities, and Mixing in Turbulent Stratified Flows. *Annual Review of Fluid Mechanics*, *53*(1), 113–145. Retrieved from `https://doi.org/10.1146/annurev-fluid-042320-` doi: 10.1146/annurev-fluid-042320-100458

Clément, L., Thurnherr, A. M., & St. Laurent, L. C. (2017). Turbulent mixing in a deep fracture zone on the Mid-Atlantic Ridge. *Journal of Physical Oceanography*, *47*(8), 1873–1896. doi: 10.1175/JPO-D-16-0264.1

Forget, G. (2010). Mapping ocean observations in a dynamical framework: A 2004-06 ocean atlas. *Journal of Physical Oceanography*, *40*(6), 1201–1221.

Ijichi, T., & Hibiya, T. (2018). Observed variations in turbulent mixing efficiency in the deep ocean. *Journal of Physical Oceanography*, *48*(8), 1815–1830. Retrieved from `www.ametsoc.org/PUBSReuseLicenses` doi: 10.1175/JPO-D-17-0275.1

Ijichi, T., St. Laurent, L., Polzin, K. L., & Toole, J. M. (2020). How Variable Is Mixing Efficiency in the Abyss? *Geophysical Research Letters*, *47*(7), 1–9. doi: 10.1029/2019GL086813

Kaminski, A. K., & Smyth, W. D. (2019). Stratified shear instability in a field of pre-existing turbulence. *Journal of Fluid Mechanics*, *862*, 639–658. doi: 10.1017/jfm.2018.973

Large, W. G., McWilliams, J. C., & Doney, S. C. (1994). Oceanic vertical mixing: A review and a model with a nonlocal boundary layer parameterization. *Reviews of Geophysics*, *32*(4), 363–403.

Lien, R.-C., Caldwell, D. R., Gregg, M. C., & Moum, J. N. (1995). Turbulence variability at the equator in the central {P}acific at the beginning of the 1991–1993 {E}l {N}ino. *J. Geophys. Res.: Oceans*, *100*(C4), 6881–6898.

Marshall, J., Adcroft, A., Hill, C., Perelman, L., & Heisey, C. (1997). A finite-volume, incompressible navier stokes model for, studies of the ocean on parallel computers. *J. Geophys. Res.*, *102*(C3), 5753–5766. doi: 10.1029/96JC02775

Mashayek, A., Ferrari, R., Merrifield, S., Ledwell, J. R., St Laurent, L., & Garabato, A. N. (2017). Topographic enhancement of vertical turbulent mixing in the Southern Ocean. *Nature communications*, *8*, 14197.

Mashayek, A., Salehipour, H., Bouffard, D., Caulfield, C. P., Ferrari, R., Nikurashin, M., ... Smyth, W. D. (2017). Efficiency of turbulent mixing in the abyssal ocean circulation. *Geophysical Research Letters*, *44*(12), 6296–6306.

Moum, J. N. (1996). Efficiency of mixing in the main thermocline. *J. Geophys. Res.*, *101*(C5), 12–57.

Osborn, T. R. (1980). Estimates of the local rate of vertical diffusion from dissipation measurements. *Journal of Physical Oceanography*, *10*, 83–89.

Polzin, K. L., Toole, J. M., Ledwell, J. R., & Schmitt, R. W. (1997). Spatial variability of turbulent mixing in the abyssal ocean. *Science*, *276*(5309), 93–96.

Portwood, G. D., de Bruyn Kops, S. M., & Caulfield, C. P. (2019). Asymptotic dynamics of high dynamic range stratified turbulence. *Phys. Rev. Lett.*, *122*, 194504.

Salehipour, H., Peltier, W. R., & Caulfield, C. P. (2018). Self-organised criticality of turbulence in strongly stratified mixing layers. *J. Fluid Mech.*, *856*, 228–256.

Smyth, W. D. (2020). Marginal instability and the efficiency of ocean mixing. *J. Phys. Oceanogr.*, *50*, 2141–2150.

Smyth, W. D., Moum, J., & Caldwell, D. (2001). The efficiency of mixing in turbulent patches: inferences from direct simulations and microstructure observations. *J. Phys. Oceanogr.*, *31*, 1969–1992.

Smyth, W. D., Nash, J. D., & Moum, J. N. (2019). Self-organized criticality in geophysical turbulence. *Sci. Reports*, *9*, 3747.

Thorpe, S., Smyth, W., & Li, L. (2013). The effect of small viscosity and diffusivity on the marginal stability of stably stratified shear flows. *J. Fluid Mech.,(submitted)*.

Tulloch, R., Ferrari, R., & others. (2014). Direct estimate of lateral eddy diffusivity upstream of Drake Passage. *Journal of Physical Oceanography*, *44*(10), 2593–2616.

van Reeuwijk, M., Holzner, M., & Caulfield, C. P. (2019). Mixing and entrainment are suppressed in inclined gravity currents. *J. Fluid Mech.*, *873*, 786?815.

Zhou, Q., Taylor, J. R., & Caulfield, C. P. (2017). Self-similar mixing in stratified plane Couette flow for varying Prandtl number. *J. Fluid Mech.*, *820*, 86–120.